

# Violation of generalized fluctuation theorems in adaptively driven steady states: Applications to hair cell oscillations

Janaki Sheth,<sup>1</sup> Dolores Bozovic,<sup>1,2</sup> and Alex J. Levine<sup>1,3,4</sup>

<sup>1</sup>*Department of Physics and Astronomy, UCLA, Los Angeles California, 90095-1596, USA*

<sup>2</sup>*California NanoSystems Institute, UCLA, Los Angeles California, 90095-1596, USA*

<sup>3</sup>*Department of Chemistry and Biochemistry, UCLA, Los Angeles California, 90095-1596, USA*

<sup>4</sup>*Department of Computational Medicine, UCLA, Los Angeles California, 90095-1596, USA*

(Dated: December 21, 2024)

We explore the correlation and response functions of stochastic nonlinear oscillators driven by internal energy-consuming processes which are in addition *adaptive*, that is their power input depends on the current state of the system. Such dynamics are observed in a variety of biological systems, including the spontaneous oscillations of hair cells of the inner ear. We propose a generalization of the well-known fluctuation-dissipation theorem (FDT) for such a steady-state non-equilibrium system by analyzing its perturbations using a co-moving reference frame that rotates along its mean limit cycle, and test the universality thereof. In particular through numerical simulations and analytical calculations, we demonstrate that for noisy systems whose steady states are modulated by adaptation, both the FDT and its generalization (GFDT) fail. Thus, testing for the experimental breakdown of the latter may provide further insight into intriguing feedback mechanisms in such dynamical systems.

## I. INTRODUCTION

Biology is replete with cyclic nonequilibrium steady state dynamics. Examples include the chemical networks underlying Cicardian rhythms, activity patterns in neuronal networks, and cardiac rhythmogenesis [1–6]. The inner ear provides another example of such dynamics [7].

An integral part of the vertebrate peripheral auditory system, the hair cells of the inner ear [8] transduce pressure waves ranging over six orders of magnitude in amplitude into electrical signals through the opening of specific ion channels in response to minute lateral displacements of a columnar structure, the stereocillium [9]. These bundles of filaments protruding from the hair cells' surface are exquisitely sensitive to displacements, allowing the cell to produce electrical signals in response to Ångstrom-scale displacements of the stereocillium bundle. While the biophysical mechanisms enabling this sensitivity are not entirely known, it is clear that internal active dynamical processes, driven by endogenous molecular motors (Myosin 1c) are essential for this sensitivity.

The force feedback mechanism depends on the state of the filament, which allows the hair cell to maintain its extreme sensitivity to incoming signals even under exogenous mechanical loading. The mechanical feedback between the myosin motors and bundle displacements has other consequences as well. It allows for an unstable dynamical regime in which the stereocillium bundle responds to mechanical input like a spring with a negative spring constant [10]. In this regime, the bundle undergoes active oscillations even in the absence of incoming pressure waves due to the active feedback between motor activity and bundle displacement. Since that endogenous drive depends on deformation of the bundle, driven hair cell provides a direct mechanical example of homeostatic control of a nonequilibrium steady state that is

common in biology, such as those found in *e.g.*, cellular regulation [12] and bacterial chemo-sensing [13].

Hair cell oscillations are quite noisy. Brownian motion of the stereocillium leads to the nanometer scale displacements [21]. Force fluctuations resulting from stochastic myosin motor activity are also present and may contribute colored-noise [21]. Finally, the membrane potential of the cell body, which is coupled to stereocillium displacement, fluctuates due to ion channel clatter and shot noise in the ionic transport through transmembrane channels [23]. As a result, the limit cycle oscillations of the hair cell bundle provide a window into the basic nonequilibrium statistical mechanics of a noisy limit cycle oscillator under homeostatic control where the drive maintaining the nonequilibrium steady state responds to the state of the system.

There are many experimental studies of this system using *in vitro* preparations [7, 10, 42]. Based on these, a set of robust mathematical models of the driven system have been developed comprising of a set of nonlinear differential equations of varying degrees of complexity [21, 24]. The simplest of which is a two-dimensional dynamical system that undergoes a supercritical Hopf bifurcation to limit cycle (oscillatory) state [27, 28]. In this manuscript, we use that spontaneously oscillating state, modeled by the stochastic Hopf equations, to study fluctuation theorems associated with such noisy nonequilibrium systems. It is well known that fundamental equilibrium fluctuation theorems can fail in nonequilibrium steady states. In fact, the breakdown of the standard fluctuation dissipation theorem (FDT) [30] has been used as a way to characterize the nonequilibrium steady state of cytoskeletal networks [36]. More recently, there has been a new exploration of fluctuation theorems applicable to nonequilibrium steady states [26]. Here we show that, as expected, the driven hair bundle violates the standard, equilibrium FDT, but does obey a generalized fluctua-

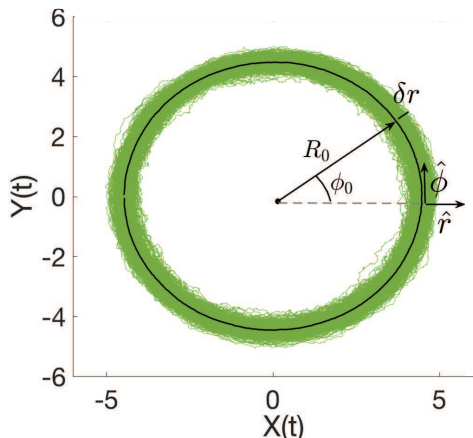


FIG. 1 (color online). A typical stochastic trajectory of a noisy Hopf oscillator based on Eq. 1 is shown in green. Its mean limit cycle is shown as the black circle, which has a particularly simple Frenet frame  $\{\hat{r}, \hat{\phi}\}$  – these unit vectors the local normal and tangent to the curve respectively.

tion dissipation theorem (GDFT), as predicted by the new body of work on fluctuation theorems in nonequilibrium steady states. This agreement with the GDFT, however is predicated on the drive being nonadaptive, meaning that the power input from the drive does not depend on the current state of the system. Once we include this feature related to the homeostatic control of the hair bundle oscillations, we obtain new violations of the nonequilibrium GDFT. We propose that, just as the violation of the original FDT in biological systems is an important quantitative measure of nonequilibrium dynamics [41], the violation of the nonequilibrium generalization of the FDT, the GFDT, should be a useful quantitative indicator of active feedback or homeostatic control in biological dynamical systems.

The simplest dynamical model of bundle oscillations is the stochastic supercritical Hopf oscillator in its normal form. This two-dimensional dynamical system can be described in terms of the complex variable  $Z(t) = x(t) + iy(t)$ , which obeys the differential equation

$$\dot{Z} = Z(\mu + i\omega) - bZ|Z|^2 + \eta(t) + f(t), \quad (1)$$

where  $f(t) = 0$  is an external deterministic force acting on this overdamped system and  $\eta(t)$  is a stochastic force, described below. The dynamics of the deterministic and unforced system ( $f = \eta = 0$ ) are controlled by the values of the model parameters  $\{\mu, \omega, b = b' - ib'', (b', b'' > 0)\}$ . The real parameter  $\mu$  determines the power input to the system. When  $\mu < 0$  this term damps the oscillator, leaving the system with a single fixed point at  $z = 0$  having an infinite basin of attraction. As this parameter becomes positive, there is positive energy input into the system so that the oscillator undergoes a supercritical Hopf bifurcation into a circular limit cycle of radius  $R_0 = \sqrt{\mu/b'}$ , which also an infinite basin of attraction. The oscillator has an angular frequency given by  $\omega_0 = \omega +$

$R_0^2 b''$ , where we assume that  $\omega$  is real.

To specify the stochastic system, we include a Gaussian white noise force  $\eta_Z = \eta_X + i\eta_Y$  with zero mean.

$$\langle \eta_i(t) \rangle = 0, \quad (2)$$

$$\langle \eta_i(t)\eta_j(t') \rangle = A_{ij}\delta(t-t'). \quad (3)$$

with  $A_{ij}$  allowing for the uncorrelated noise in the  $x, y$  channel to be drawn in principle from different Gaussian distributions. Finally, we include deterministic external perturbations via  $f_Z(t) = f_x(t) + if_y(t)$ .

Trajectories derived from Eq. 1 are those of an overdamped particle moving in two dimensions in response to a force field  $\mathbf{f}$ , which can be decomposed into the gradient of an azimuthally symmetric scalar potential energy  $\Phi(r)$  and a vector potential  $\mathbf{A} = \hat{z}A(r)$ ,

$$\Phi(r) = -\frac{\mu}{2}r^2 + \frac{b'}{4}r^4, \quad (4)$$

$$A(r) = -\frac{\omega}{2}r^2 - \frac{b''}{4}r^4 \quad (5)$$

where here in the following it will be convenient to work in polar coordinates:  $x_r = r = \sqrt{x^2 + y^2}$  and  $x_\phi = \phi = \arctan(y/x)$  [25]. The conservative system with  $\omega = b'' = 0$  when driven by white noise corresponds to the case of the overdamped particle in thermal equilibrium at some noise temperature. The vector potential, representing the action of the hair cell's endogenous molecular motors, does work on the overdamped system, generating the limit cycle oscillations as shown in Fig. 1 using parameters:  $\mu = 40, \omega = 10, b' = 2, b'' = 2$ . The other simulation details are standard and described in Appendix B. The appearance of a force field produced by a vector potential does not alone generate a limit cycle or even a nonequilibrium steady state. The necessary and sufficient conditions to create such a state with a time-independent force field is that the force field is proportional to curl of a vector potential and that the force does work on the particle representing the state of the oscillator in our case. A classic counter example where the second condition is not met is provided by a charged particle in a magnetic field. In Appendix A we review this case, showing a damped, charged particle in a two dimensional harmonic potential and in a uniform applied magnetic field aligned in the direction perpendicular to the plane of the charged particle's motion obeys the standard FDT even in the presence of the magnetic field.

More generally, for hair cell models, one allows the  $b$  coefficient to be complex, as mentioned above. In this case, the azimuthal drive generates dynamics of the form  $\dot{\phi} = r^{-1}\nabla \times \mathbf{A} = \omega + b''r^2$ . The power input of the drive is now *adaptive*, meaning that the work it does on the particle depends on the current state of the system through the radial coordinate. In the hair cell literature, when the azimuthal coordinate is driven independently of the state of the system as given by  $r$ , i.e., when  $b'' = 0$ , the system is said to experience isochronous driving. Conversely, adaptive driving where  $b'' \neq 0$  are referred to as

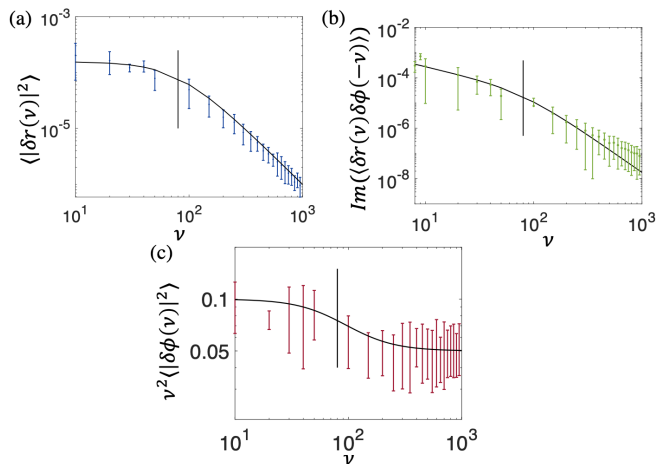


FIG. 2 (color online). Colored points represent the power spectrum as a function of frequency  $\nu$  of two point correlations between deviations of the radius (a), cross correlations between deviations of the radius and the phase (b), and the phase (c). Data points were obtained from numerical simulations described in the text and the error bars denote the standard deviation of the mean. The corner frequency of the Lorentzian radial autocorrelations is marked by a vertical (black) line. The coupling of  $\delta r$  to  $\delta \phi$ , is seen in the change in the cross-correlation of (b) and the frequency-dependent phase diffusion constant (plotted in c) at the same frequency, also demarcated by vertical lines. Superposed on each curve (black lines) is the analytic prediction discussed in the text – see Eq. 14.

nonisochronous drives. For our purposes, the important feature of this model is that the adaptation of the drive forcing the steady-state limit cycle oscillations can be continuously varied through that one model parameter  $b''$ .

To study the fluctuations of the system about its limit cycle (when  $\mu > 0$ ), we expand about the limit cycle

$$r(t) = R_0 + \delta r(t), \quad (6)$$

$$\dot{\phi}(t) = \omega_0 + \delta \dot{\phi}(t). \quad (7)$$

to find two coupled stochastic linear Langevin equations for the fluctuations of the radius  $\delta r$  and phase  $\delta \phi$  of the

oscillator

$$\delta \dot{r} = -2\mu \delta r + \eta_r + f_r, \quad (8)$$

$$\delta \dot{\phi} = 2b'' \sqrt{\frac{\mu}{b'}} \delta r + \eta_\phi + f_\phi. \quad (9)$$

Here, the terms  $\{\eta_r, \eta_\phi\}$  and  $\{f_r, f_\phi\}$  are projections of the stochastic and perturbative forces respectively onto the local normal  $\hat{r}$  and tangent  $\hat{\phi}$ . These unit vectors span the Frenet-Serret frame associated with the deterministic limit cycle being the normal and tangent directions respectively. The Frenet-Serret frame advances and simultaneously rotates along the deterministic curve at the angular velocity  $\omega_0$ . By working in this co-moving reference frame, we effectively subtract away the mean non-equilibrium dynamics of the steady-state oscillator and by doing so allows us to recover a generalized fluctuation-dissipation theorem (GFDT) for the nonequilibrium system, as discussed by Seifert and coworkers [16]. The use of the dimensionless phase angle  $\phi$  instead of the arclength variable  $s = R_0\phi$  requires the noise amplitudes  $\eta_{r,\phi}$  have different length dimensions. We account for this explicitly in the following, we set second moments of the Gaussian force fluctuations in the frequency domain to be

$$\langle |\eta_r(\nu)|^2 \rangle = 1 \quad (10)$$

$$\langle |\eta_\phi(\nu)|^2 \rangle = R_0^{-2}, \quad (11)$$

$$(12)$$

which also has the effect of setting the effective noise temperature to  $1/2$  since the mobilities in the Hopf equation have been set to unity. To account for this dimensional difference, it will be convenient in the following to define a symmetric “temperature matrix” by  $\mathcal{T}_{rr} = 1, \mathcal{T}_{r\phi} = R_0^{-1}, \mathcal{T}_{\phi\phi} = R_0^{-2}$ . This choice of coordinates has no other consequences for our analysis.

To verify the GFDT in the co-moving frame, we first compute the correlation matrix in the frequency domain

$$\mathcal{C}(\nu) = \begin{bmatrix} \langle |\delta r(\nu)|^2 \rangle & \langle \delta r(\nu) \delta \phi(-\nu) \rangle \\ \langle \delta \phi(\nu) \delta r(-\nu) \rangle & \langle |\delta \phi(\nu)|^2 \rangle \end{bmatrix}. \quad (13)$$

from Eqs. 8, 9 and obtain

$$\mathcal{C}(\nu) = \begin{bmatrix} \frac{1}{4\mu^2 + \nu^2} & 0 \\ 0 & \frac{1}{\nu^2} \end{bmatrix} + 2b'' \begin{bmatrix} 0 & \frac{-i}{\nu(4\mu^2 + \nu^2)} \\ \frac{i}{\nu(4\mu^2 + \nu^2)} & \frac{2b''}{\nu^2(4\mu^2 + \nu^2)} \end{bmatrix} \quad (14)$$

The radial autocorrelations are those of an overdamped harmonic oscillator, as expected from the form of the scalar potential Eq. 4 near the circular limit cycle  $r = R_0$ . Similarly, the autocorrelations of the phase angle  $\sim \nu^{-2}$ , reflect phase diffusion. When the drive is nonadaptive or isochronous  $b'' = 0$  there is a simple, frequency-

independent phase diffusion constant and there are no cross correlations between the radial and phase fluctuations. The adaptation of the drive, however, introduces both a frequency-dependent phase diffusion constant (observed in hair-cell data [27]) and more importantly new correlations between the radial and phase fluctuations.

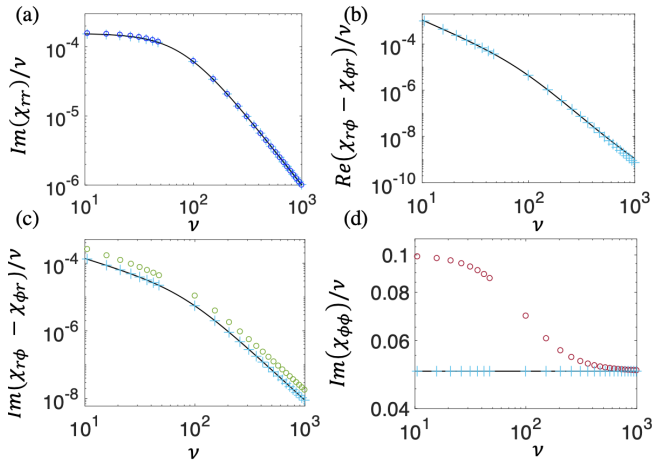


FIG. 3 (color online). Breakdown of the generalized fluctuation dissipation theorem for the Hopf oscillator. We plot the response functions as measured from our simulations (light blue crosses), determined by our analytic predictions (black lines) and inferred from the direct application of the GFDT (circles). GFDT violations are seen in the divergence of these circles and both the calculated or measured response functions. No violations are seen in the radial variable (a), but significant deviations appear in GFDT-predicted correspondence between the phase fluctuations and response function (d). In panels (b) and (c) we show the real and imaginary parts of the cross response between the radial and phase degrees of freedom. Due to the unidirectionality of the coupling between these variables  $\chi_{\phi r} \neq \chi_{r\phi} = 0$ .

Both of these effects arise because the external drive now responds to the state of system as documented by  $\delta r$  by changing its power input. All three correlation functions are shown in Fig. 2, where the solid (black) lines show the theoretical predictions and the (colored) points the measured results from our Brownian simulations. The error bars on the numerical data points represent the standard deviation of the mean.

A direct calculation of the response matrix  $x_\alpha(\nu) = \chi_{\alpha\gamma}(\nu)f_\gamma(\nu)$  gives

$$\chi(\nu) = \begin{bmatrix} 0 & 0 \\ -2b'' \sqrt{\frac{\mu}{b'}} \frac{1}{\sqrt{2\mu - i\nu}} \frac{1}{(i\nu)(2\mu - i\nu)} & -\frac{1}{i\nu} \end{bmatrix}. \quad (15)$$

We define the deviation matrix from the GFDT as

$$\Delta_{\alpha\beta}(\nu) = [\chi_{\alpha\beta}(\nu) - \chi_{\beta\alpha}(-\nu)] \mathcal{T}_{\beta\gamma} - 2i\nu \mathcal{C}_{\alpha\gamma}(\nu), \quad (16)$$

and find that deviations from the GFDT (FDT in the co-moving frame associated with the deterministic limit cycle) appear only in the presence of an adaptive or homeostatic drive  $b'' \neq 0$ :

$$\Delta(\nu) = 2b'' \begin{bmatrix} 0 & \sqrt{\frac{\mu}{b'}} \frac{(-\nu + 2i\mu)}{(4\mu^2\nu + \nu^3)} \\ \sqrt{\frac{\mu}{b'}} \frac{(\nu + 2i\mu)}{(4\mu^2\nu + \nu^3)} & \frac{2b''}{\nu^2(4\mu^2 + \nu^2)} \end{bmatrix}. \quad (17)$$

Only the Lorentzian fluctuations of the radial  $\delta r$  variable obey the GFDT when the drive is adaptive. When

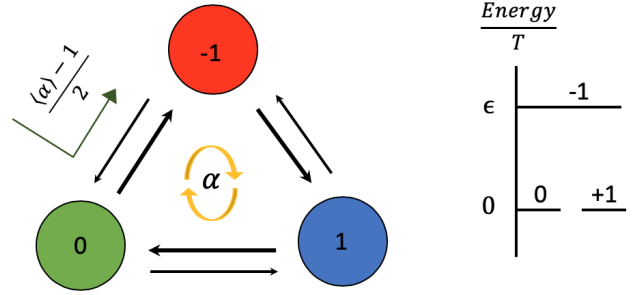


FIG. 4 (color online). A schematic diagram of the three-state system, showing states  $\{-1, 0, 1\}$  denoted by red, green and blue disks respectively. These states have energies  $\{\epsilon, 0, 0\}$ . In the nonequilibrium steady state the clockwise transitions rates are enhanced over their detailed-balance values by  $\alpha(t)$ . The resulting steady-state probability current may be removed by working in a co-moving frame.

$b'' \neq 0$  the feedback between the azimuthal driving force and the radial oscillations breaks the GFDT due to both new cross correlations  $C_{r\phi}$  and a modified phase diffusion  $C_{\phi\phi}$ . This breakdown of the GFDT cannot be removed by an appropriate change of variables, as has been explored for nonequilibrium fluctuations about a fixed point [20]. Turning back to our numerical simulations we show in Fig. 3(a) the correspondence between the measured response (light blue cross) and that expected from the correlation function (dark blue circle) in the radial variable based on the GFDT, ( $\Delta_{rr} = 0$ ). In Fig. 3(b) and 3(c) we show the real and imaginary parts of the off-diagonal response function, giving the phase response to a radial force  $\chi_{\phi r}$ . Here, the other off-diagonal component, giving the radial response to an azimuthal force  $\chi_{r\phi}$  (advancing the phase of the oscillator) vanishes. The cross-correlation predicts only an imaginary component (green circle). Finally, in Fig. 3(d), we show the phase diffusion constant measured from the numerical simulation (blue cross) and the prediction of that diffusion constant based on the GFDT (red circle). Clear deviations are observed at low frequency due to the adaptive drive, as predicted by Eq. 17. When adaptation is removed (see Fig. 9 in supplemental materials), these deviations vanish and the full GFDT is restored.

To better understand the role of adaptive feedback on the drive in breaking GFDT, it is helpful to examine the same phenomenon in a more simple, finite-state model. As shown in Fig. 4 consider a system with three states labeled by  $s = \{-1, 0, +1\}$  having energies  $\{\epsilon, 0, 0\}$ . The stochastic dynamics of the system is defined by a discrete time master equation for the probability  $p_n(t)$  of observing the system in state  $n$  at time  $t$

$$p_n(t_{i+1}) = \sum_{m \neq n} [p_m(t_i) \alpha_{mn}(t_i) - p_n(t_i) \alpha_{nm}(t_i)], \quad (18)$$

which depends on six transition probabilities, *e.g.*, the transition rate from state  $n$  to  $m$  at time  $t_i$ :  $\alpha_{nm}(t_i)$ .

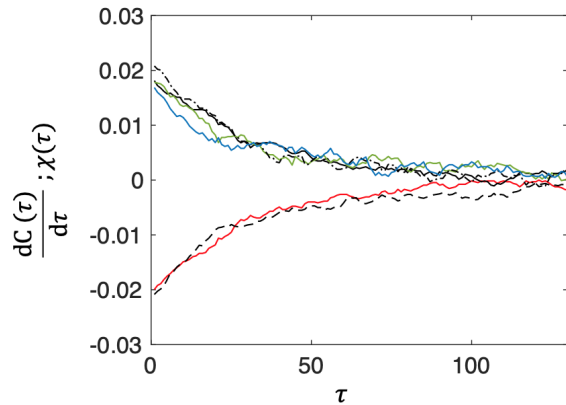


FIG. 5 (color online). Testing the FDT with detailed balance:  $\alpha(t) = 1$ . By comparing  $\frac{dC_{-1-1}}{d\tau}$  (black dashed line) and  $\chi_{-1-1}$  (red line), we check that the response of the system to a force driving it out of the  $-1$  state matches the appropriate correlation function derivative. We also find the expected correspondence between  $\frac{dC_{0-1}}{d\tau}$  (black solid line) and  $\chi_{0-1}$  (green line) as well as  $\frac{dC_{1-1}}{d\tau}$  (black dashed-dot line) and  $\chi_{1-1}$  (blue line).

These six transition probabilities are given by the following rules. We set

$$\alpha_{nm} = \alpha_{mn} e^{\epsilon_n - \epsilon_m} \alpha(t_i) \quad (19)$$

where  $n$  is to the right of  $m$  in the list of states  $\{-1, 0, 1\}$  or its cyclic permutations. The factor  $\alpha(t_i)$  allows us to drive the system into a nonequilibrium steady-state by breaking detailed balance. By choosing  $\alpha$  to be a constant greater than one, we generate a clockwise probability current – see Fig. 4 – in steady state. Such a choice is analogous to turning on a non-adaptive drive in the isochronous Hopf model ( $w \neq 0$ ) of the hair cell oscillator. To introduce adaptation, we also consider the case in which the drive depends on a sum over the history of the system by setting

$$\alpha(t_i) = 1 + r \sum_{j=1}^{\infty} e^{\lambda(i-j)} \sigma(t_{i-j}), \quad (20)$$

where  $\sigma(t_k)$  is an indicator function taking values  $\pm 1$  or  $0$  if the system is in that state at time  $t_k$ . The strength of the adaptation is controlled by  $r$ , which determines the change in the drive, and  $\lambda$ , which controls the exponential decay rate of the memory kernel in Eq. 20. It is measured in inverse time units  $\delta t = t_{i+1} - t_i$ , which we always set to  $10^{-2}$ . The effect of the adaptation is to increase the drive when the system has recently been  $+1$  state and decrease it when the system has visited the  $-1$  state.

We first performed numerical simulations of the symmetric three-state model, i.e.,  $\epsilon = 0$  and detailed balance ( $\alpha = 1$ ), tracking the stochastic trajectories of 50 realizations of the system over a total of  $2 \times 10^4$  time steps for each of the realizations. For additional details of these

simulations we refer the reader to Appendix B. The occupation probability of the three states was one third as expected (not shown). From these trajectories we may compute all two-point correlation functions

$$C_{nm}(\tau) = \frac{1}{2} [\langle \sigma_n(t_i + \tau) \sigma_m(t_i) \rangle + \langle \sigma_m(t_i + \tau) \sigma_n(t_i) \rangle] \quad (21)$$

The average is taken over an ensemble of trajectories at time delay  $\tau$ . Under the assumption of ergodicity, we one may alternatively average over longer time series from one trajectory. Our definition of the correlation function was chosen to make the correlation function explicitly time reversal invariant when  $n \neq m$ . We do so under the assumption that one investigating the stochastic dynamics of a complex nonequilibrium steady state might implicitly assume time reversal invariance. Clearly, if the driven system admits a non-vanishing probability current, this symmetry will not be valid. Since we propose the use of the violation of fluctuation theorems as a test for both an underlying limit cycle in general and an adaptively driven one in particular, we do not suppose *a priori* that the correlation data are collected under any assumptions regarding the time reversal invariance of the system.

To test the standard fluctuation-dissipation theorem, we numerically obtained the response function of the system to a force conjugate to the occupation of state  $-1$ ,

$$\delta p_n(t_i) = - \sum_{j=-\infty}^i \chi_{n-1}(t_i - t_j) \delta \epsilon_{-1}(t_j), \quad (22)$$

by setting the energy of that state to  $\epsilon_{-1} = 3$  for one time step and observing the subsequent stochastic evolution of the system. In Fig. 5 we plot  $\chi_{-1-1}(\tau)$ ,  $\chi_{0-1}(\tau)$ , and  $\chi_{1-1}(\tau)$  as solid red, green, and blue curves respectively. As expected, the transient increase in the energy of the  $-1$  state suppresses its occupation probability of that state and symmetrically increases the occupation probability of the other two states:  $+1$  and  $0$ . The system recovers its equilibrium probabilities exponentially with a decay rate of about 30 inverse time units. The standard fluctuation dissipation theorem requires that these response functions must be equal to the time derivative of the correlation functions  $dC_{n-1}/d\tau(\tau)$  evaluated at time delay  $\tau$  with  $n = -1, 0$  and  $1$  respectively. We plot the numerically obtained time derivatives of the correlation functions  $C_{-1-1}$ ,  $C_{0-1}$  and  $C_{1-1}$  as dashed black, solid black and dashed-dot black lines respectively. As expected, we find that the time derivatives of the correlation functions of the occupation of the states agrees with the response of the occupation probability to a force conjugate to that variable. All the correlation functions in this figure were normalized such that  $C_{nm}(0) = 1$ . The response functions were multiplied by an empirical temperature, in this case 0.125. Upcoming computations from this system are similarly normalized.

We now repeat this measurement in a non-equilibrium system by setting  $\alpha = 98$ . This choice of a *non-adaptive* drive breaks detailed balance and is analogous to the

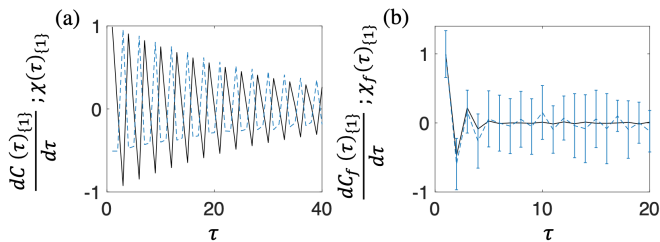


FIG. 6 (color online). (a) FDT violations with broken detailed balance at  $\alpha = 98$ . We compare the time derivative of the cross-correlation  $C_{1-1}$  (black line) and the response function  $\chi_{1-1}$  (blue dashed line). (b) Working in a co-moving frame chosen so there is no net steady-state probability current we obtain a generalized FDT (GFDT). Now the time derivative of the  $C_{1-1}$  (black line) agrees with the corresponding response function (dashed blue line). Error bars denote the standard deviation of the mean. Due to symmetry, we show only one set of response and correlation functions.

Hopf model of hair cell oscillations with  $b'' = 0$  but  $\omega > 0$ . In Fig. 6a we show measured response function  $\chi_{1-1}(\tau)$ . As in the equilibrium case, the applied force pushes the system out of the  $-1$  state into the  $0, 1$  states. But, unlike the equilibrium case, the change in probability oscillates in time due to the detailed-balance-breaking drive. For example, the occupation probability of  $+1$  cycles the three state system in the clockwise direction while slowly decaying over longer times (not shown) resulting in an oscillatory response function shown as the dashed blue line in the figure. The correlation function  $C_{1-1}(\tau)$  also shows this oscillatory behavior, but its derivative (black line) *does not* match the corresponding response function. The standard fluctuation dissipation theorem is violated.

We can, however, restore a generalized fluctuation dissipation theorem in the driven system by working in a “rotating” reference frame – one that moves with the clockwise probability current of the non-equilibrium steady state at fixed  $\alpha \neq 1$ . This is done by defining new state occupation variables

$$\tilde{\sigma}_k(t_i) \equiv \sigma(t_i) \pmod{3} \quad (23)$$

After doing so, we now find that the response function of the  $+1$  state in the co-rotating frame to a force acting on the  $-1$  state – the dashed blue line in Fig. 6b now agrees with the numerically measured time derivative of the correlation function, shown as the black line in this figure. The error bars represent the standard deviation of the mean for the response data. We find a similar agreement between the other correlation and response functions in the co-rotating frame; these are shown in appendix B (Figs. 10 and 11). While neither the time derivative of the correlation function nor the response function in the driven system agree with predictions based on the equilibrium system, their agreement with each other shows that a generalized fluctuation dissipation theorem holds in the driven system, as expected based on the work of

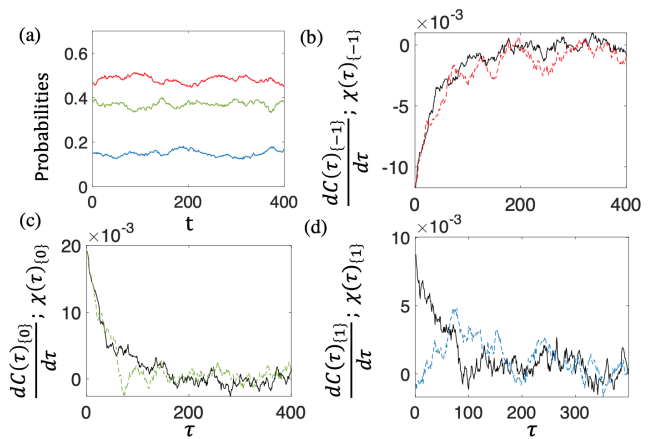


FIG. 7 (color online). The three-state system with an adaptive drive, Eq. 20. (a) With the adaptive drive at  $r = 0.095$  and  $\lambda = 0.1$ , the states are no longer occupied with equal probability even when their occupation energies are equal. In panels (b)-(d) we compare  $\frac{dC}{dt}$  (black solid) with the appropriate  $\chi$  (color) in the ground frame. In one case (d) we observe significant deviations from the FDT.

the Seifert and collaborators. The appearance of the GFDT in the co-rotating frame, which zeros out the steady-state probability current of the driven system, is analogous to our observation of a similar fluctuation theorem in the driven Hopf oscillator system without the adaptive drive, i.e., with  $b'' = 0$ .

We now include drive adaptation in the three-state model using Eq. 20 which breaks detailed balance by introducing a memory kernel dependent on previous state occupation. This is homologous to the non-isochronous Hopf model with  $b'' > 0$  and  $\omega = 0$  – thus disentangling the two force fields. Choosing  $r = 0.095$  and a memory time of approximately ten time steps  $\lambda = 0.1$ , we now obtain a steady-state system with non-equal occupation probabilities of the three states in steady state. In spite of the fact that the energies of all three states are equal, the adaptive drive breaks the permutation symmetry of these states as shown in panel a of Fig. 7. As a result the simple occupation probabilities of the states in this nonequilibrium steady state do not reflect their relative energies. Conversely, just by observing these occupation probabilities, one might conclude erroneously that this system was in equilibrium with a particular spectrum of energy levels. To test this conclusion, one must not only examine these probabilities but also compare correlation and response functions of the system.

In the three remaining panels (b-d) of Fig. 7, we show a comparison of the time derivative of the correlation function  $\dot{C}_{k-1}(\tau)$  and the response function  $\chi_{k-1}(\tau)$  for  $k = -1, 0, +1$  in panels b, c, and d respectively. The standard FDT fails vividly for one set of measurements:  $C_{1-1}(\tau) \neq \chi_{1-1}(\tau)$  over the range of time delays for which these two quantities differ from zero – see Fig. 7d.

Time variability of the steady state probability cur-

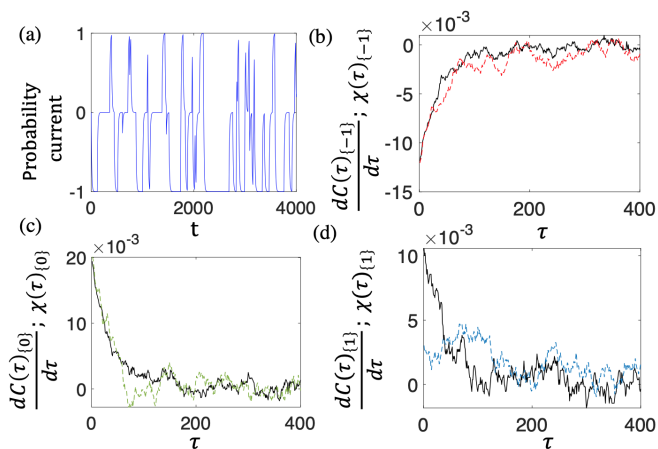


FIG. 8 (color online). (a) The steady-state probability current  $\alpha(t_i) - 1$ . Panels (b)-(d) illustrate the violation of GFDT as we compare the derivatives of the correlation functions and the corresponding  $\chi$ s in the comoving frame.

rent of this three-state model is illustrated in Fig. 8a. Observing from the co-rotating frame – whose velocity is half of the time-average value of this current – according to GFDT, the time derivative of the corresponding correlation function (black line) and the response function (colored line) should match. They do within the precision of our numerical measurements for  $k = -1, 0$  (panels b and c), but the generalized theorem is violated for the state 1 (Fig. 8d). The adaptation of the driving force maintaining the nonequilibrium steady state in this simple, three-state system is clearly revealed by the failure of the GFDT, just as the nonisochronous drive with  $b'' > 0$  breaks the analogous GFDT in the driven Hopf oscillator.

## II. DISCUSSION

The simplest hair cell model presents an interesting stochastic dynamical system allowing one to explore fluctuation theorems in nonequilibrium steady states. It is well known that such nonequilibrium steady states can violate the fluctuation dissipation theorem. In fact, the failure of that theorem has been used as a test for and measure of the nonequilibrium nature of various stochastic steady-states. There are, however, multiple ways to violate the FDT. For example in actomyosin gels, one observes enhanced strain fluctuations at low frequencies due to motor activity. This is a consequence of the fact that the motor dynamics introduce experimentally relevant time scales thereby producing force autocorrelations with a colored noise spectrum. As a result, the strain fluctuations do not correspond to the (visco-)elastic system at any temperature. One outcome of this analysis and that of related systems is that one can use the breakdown of the FDT as a type of sensor tuned to the detection of

nonequilibrium steady states. Often in complex biological systems, such a tool is useful.

In this article, we consider a different class of nonequilibrium systems, which break the FDT: those driven into stochastic steady states characterized by a stationary probability current and broken detailed balance. In this case, previous work has introduced a new class of generalized fluctuation theorems based on working in a co-moving reference frame that zeroes out the stationary probability current. When fluctuations are now viewed in that frame there is a familiar relation between them and the response function(s) of the system. The simplest hair cell model provides an example of such a stochastic driven system; our previous work on fluctuations in a Frenet frame co-moving with the mean probability current of the system reproduced the expected GFDT. This model, however, introduces a new complication – an adaptive drive: the internal drive maintaining the nonequilibrium steady state in effect measures the state of the system and adapts its power input based on that measurement.

We first observed in the Hopf hair cell oscillator model with adaptive drive, the violation of GFDT. Moreover, the quantitative degree of that violation is proportional to a single model parameter  $b''$  controlling the degree of adaptation of the drive, as shown by our analytic results. To isolate this feature of drive adaptation in an even simpler system, we introduced a three state system defined by a discrete time master equation. By introducing a violation of detailed balance, we produced states with a nonzero probability current. These violate the standard FDT, as expected. Moreover, by introducing a co-rotating frame to zero the probability current in the three-state system we obtain a GFDT, as is consistent with previous work. But when we introduce drive adaptation by allowing the probability current to adjust based on the history of the system's trajectory, we once again observe the breakdown of the GFDT.

Based on this work, we propose that just as the failure of the FDT has been used to test for nonequilibrium steady states, one should be able to look for the breakdown of the GFDT as a test of stochastic steady states driven out of equilibrium by an adaptive drive. Two emblematic features of living systems are long-lived nonequilibrium steady states and homeostasis. One method to maintain homeostatic control of driven states is through an adaptive drive, as seen in the nonisochronous hair cell model. Other example of a similar homeostatic control through an adaptive drive may not be as readily apparent in complex biological systems. We propose that one may use the breakdown of the GFDT as a tool to look for them.

## ACKNOWLEDGMENTS

AJL acknowledges partial support from NSF-DMR-1709785. D.B. acknowledges support from NSF PoLS grant 1705139.

- 
- [1] E. Bunning, ed., *Biological Clocks: Cold Spring Harbor Symposium on Quantitative Biology 25* (SIAM, 1960).
- [2] A. Goldbeter, Proceedings of the Royal Society London B **261**, 319 (1995).
- [3] T. Mori, B. Binder, and C. H. Johnson, Proceedings of the National Academy of Sciences **93**, 10183 (1996).
- [4] A. Goldbeter, Nature **420**, 238 (2002).
- [5] E. M. Izhikevich, *Dynamical Systems in Neuroscience: The Geometry of Excitability and Bursting*, 1st ed. (MIT Press, Boston, 2007).
- [6] D. J. Schwab, R. F. Bruinsma, J. L. Feldman, and A. J. Levine, Physical Review E **82**, 051911 (2010).
- [7] A. J. Hudspeth, Neuron **59**, 530 (2008).
- [8] M. LeMasurier and P. Gillespie, Neuron **48**, 403 (2005).
- [9] M. Vollrath, K. Kwan, and D. Corey, Annual Rev Neurosci **30**, 339 (2007).
- [10] P. Martin, A. D. Mehta, and A. J. Hudspeth, Proceedings of the National Academy of Sciences **97**, 12026-31 (2000).
- [11] M. Benser, R. Marquis, and A. Hudspeth, J Neurosci **16**, 5629 (1996).
- [12] L. K. Nguyen J R Soc. Interface **9**, 1998-2010 (2012).
- [13] G. Lan, P. Sartori, S. Neumann, V. Sourjik and Y. Tu, Nature Physics **8**, 422-428 (2012).
- [14] L. Dinis, P. Martin, J. Barral, J. Prost, and J. F. Joanny, Phys. Rev. Lett. **109**, 160602 (2012).
- [15] J. Prost, J. F. Joanny, and J. M. R. Parrondo, Phys. Rev. L **103**, 090601 (2009).
- [16] T. Speck, and U. Seifert, Europhys. Lett. **74**, 391-396 (2006).
- [17] V. M. Eguíluz, M. Ospeck, Y. Choe, A. J. Hudspeth, and M. O. Magnasco, Phys. Rev. Lett. **84**, 5232 (2000).
- [18] A. Kern and R. Stoop, Phys. Rev. Lett. **91**, 128101 (2003).
- [19] S. Camalet, T. Duke, F. Jülicher, and J. Prost, Proceedings of the National Academy of Sciences **97**, 3183 (2000).
- [20] J. Prost, J.-F. Joanny, and J. M. R. Parrondo, Phys. Rev. Lett. **103**, 090601 (2009).
- [21] B. Nadrowski, P. Martin, and F. Jlicher, Proceedings of the National Academy of Sciences **101**, 12195 (2004).
- [22] A. D. Dorval, The Neuroscientist **12**, 442 (2006).
- [23] P. Läuger, Biochemica et Biophysica Acta – Biomembranes **413**, 1 (1975).
- [24] R. M. Amro and A. B. Neiman, Phys. Rev. E **90**, 052704 (2014).
- [25] J. Sheth, D. Bozovic, and A. Levine, Phys. Rev. E **99**, 062124 (2019).
- [26] U. Seifert, Rep. Prog. Phys. **75**, 126001 (2012).
- [27] J. Sheth, S.W.F. Meenderink, P. Quinones, D. Bozovic and A. Levine, Physical Review E **97**, 062411 (2018).
- [28] A. J. Hudseph, Nature Reviews Neuroscience **15**, 600-19 (2014).
- [29] U. Seifert, and T. Speck, European Physical Letters **89**, 10007 (2010).
- [30] H. B. Callen, and T. A. Welt, Physical Review **83**, 34-40 (1951).
- [31] R. Kubo, Reports on Progress in Physics **29**, 255 (1966).
- [32] T. S. Grigero, and N. E. Israeloff, Phys. Rev. L **83**, 5038-5041 (1999).
- [33] J. Barrat, and L. Berthier, Phys. Rev. E **63**, 012503 (2000).
- [34] M. Fuchs, and M. Cates, Journal of Physics: Condensed Matter **17**, S1681-S1696 (2005).
- [35] L. F. Cugliandolo, J. Kurchan, and L. Peliti, Phys. Rev. E **55**, 3898-3914 (1997).
- [36] D. Mizuno, C. Tardin, C. F. Schmidt, and F. C. MacKintosh, Science **315**, 370-3 (2007).
- [37] T. Betz, M. Lenz, J. F. Joanny, and C. Sykes, Proceedings of the National Academy of Sciences **106**, 15320-25 (2009).
- [38] P. Martin, A. J. Hudspeth, and F. Jülicher, Proceedings of the National Academy of Sciences **98**, 14380 (2001).
- [39] P. Martin, and A. J. Hudspeth, Proceedings of the National Academy of Sciences **96**, 14306-14311 (1999).
- [40] M. Guo, A. Ehrlicher, M. Jensen, M. Renz, J. Moore, R. Goldman, J. Lippincot-Schwartz, F. Mackintosh and D. Weitz, Cell **158**, 822-832 (2014).
- [41] F. S. Gnesotto, F. Mura, J. Gladrow, and C. P. Broedersz, Reports on Progress in Physics **81**, 066601 (2018).
- [42] P. Martin, D. Bozovic, Y. Choe, and A. J. Hudspeth, Journal of Neuroscience **23**, 4533-4548 (2003).

## Appendix A: Electrically-charged particle in a magnetic field

The motion of a damped, harmonically bound charged particle of mass  $m$  and charge  $e$  in the  $xy$  plane under the influence of magnetic field  $H\hat{z}$  is given by,

$$\ddot{\hat{r}} + \gamma\dot{\hat{r}} + \omega_0^2\hat{r} = \frac{e}{mc}\dot{\hat{r}} \times H \quad (\text{A1})$$

$$\begin{bmatrix} x \\ y \end{bmatrix} = \frac{1}{(-\omega^2 + \omega_0^2 - i\omega\gamma)^2 - \omega_r^2\omega^2} \times \begin{bmatrix} -\omega^2 + \omega_0^2 - i\omega\gamma & -i\omega_r\omega \\ i\omega_r\omega & -\omega^2 + \omega_0^2 - i\omega\gamma \end{bmatrix} \begin{bmatrix} \eta_x \\ \eta_y \end{bmatrix} \quad (\text{A5})$$

When considering these as Langevin equations, we assume rotationally symmetric thermal noise so that  $\langle \eta_x^2 \rangle = \langle \eta_y^2 \rangle = \langle \eta^2 \rangle$ .

Since the dynamics in directions  $\hat{x}$  and  $\hat{y}$  are symmetric, we compute and compare one of each of the autocorrelation and cross-correlation functions. A lengthy but

where  $\gamma$  is the friction coefficient,  $\omega_0^2$  is the natural frequency of the oscillator ( $\omega_0 = \sqrt{k/m}$  for a Hookean spring constant  $k$ ) and  $c$  the speed of light. The equations of motion may be written in terms of  $x$  and  $y$  as

$$\ddot{x} + \gamma\dot{x} + \omega_0^2x = \frac{eH}{mc}\dot{y}, \quad (\text{A2})$$

$$\ddot{y} + \gamma\dot{y} + \omega_0^2y = -\frac{eH}{mc}\dot{x} \quad (\text{A3})$$

with introduction of the classical Larmor  $\omega_r = \frac{eH}{mc}$ . Upon driving Eqs. A2 and A3 using either stochastic or deterministic (externally applied) forces we obtain:

straightforward calculation yields the following response and correlation functions. In order to confirm the validity of the FDT, we present the response functions in combinations such that these combinations should be directly equal to the corresponding response function. We find:

$$\frac{\tilde{\chi}_{xx}(\omega) - \tilde{\chi}_{xx}(-\omega)}{2i} = \frac{\gamma\omega((\omega_0^2 - \omega^2)^2 + \gamma^2\omega^2 + \omega_r^2\omega^2)}{(\omega^2\gamma^2 + (\omega_0^2 - \omega^2 - \omega\omega_r)^2)(\omega^2\gamma^2 + (\omega_0^2 - \omega^2 + \omega\omega_r)^2)} \quad (\text{A6})$$

$$C_{xx} = \frac{\langle \eta^2 \rangle ((\omega_0^2 - \omega^2)^2 + \gamma^2\omega^2 + \omega_r^2\omega^2)}{(\omega^2\gamma^2 + (\omega_0^2 - \omega^2 - \omega\omega_r)^2)(\omega^2\gamma^2 + (\omega_0^2 - \omega^2 + \omega\omega_r)^2)} \quad (\text{A7})$$

$$\frac{\tilde{\chi}_{xy}(\omega) - \tilde{\chi}_{yx}(-\omega)}{2i} = \frac{i\omega_r\omega(\omega_r^2\omega^2 - (-\omega^2 + \omega_0^2 + i\omega\gamma)^2 + (-\omega^2 + \omega_0^2 - i\omega\gamma)^2 - \omega_r^2\omega^2)}{2(\omega^2\gamma^2 + (\omega_0^2 - \omega^2 - \omega\omega_r)^2)(\omega^2\gamma^2 + (\omega_0^2 - \omega^2 + \omega\omega_r)^2)} \quad (\text{A8})$$

$$= \frac{\gamma\omega(2i\omega^3\omega_r - 2i\omega_0^2\omega\omega_r^2)}{(\omega^2\gamma^2 + (\omega_0^2 - \omega^2 - \omega\omega_r)^2)(\omega^2\gamma^2 + (\omega_0^2 - \omega^2 + \omega\omega_r)^2)} \quad (\text{A9})$$

$$C_{xy} = \frac{\langle \eta^2 \rangle (2i\omega^3\omega_r - 2i\omega\omega_r\omega_0^2)}{(\omega^2\gamma^2 + (\omega_0^2 - \omega^2 - \omega\omega_r)^2)(\omega^2\gamma^2 + (\omega_0^2 - \omega^2 + \omega\omega_r)^2)} \quad (\text{A10})$$

By direct comparison of Eqs. A6, A7, as well as the cross correlations Eqs. A8 and A10, we demonstrate that FDT for a system responding to a magnetic field. Even though the force is generated from the curl of a vector potential (like our driving force in the Hopf system), the magnetic field does not invalidate the FDT since the magnetic forces cannot do work on the system.

## Appendix B: Simulation details

The stochastic and externally perturbed Hopf oscillator of Eq. 1 was simulated using the 4<sup>th</sup>- order Runge-Kutta method for a duration of 60s, with a time step of  $10^{-4}$ s. We explore a large range in the amplitude of the noise variance  $\langle \eta_Z^2 \rangle$  covering  $10^{-7}$  to 0.4. We also used perturbative forces over a range from  $10^{-3}$  to  $10^{-1}$ . The amplitude of mean limit cycle oscillators was held to be  $O(1)$ . While consistent results were obtained over the full span of these values, Figs. 2 and 3 employ the highest value of force and noise in their respective ranges.

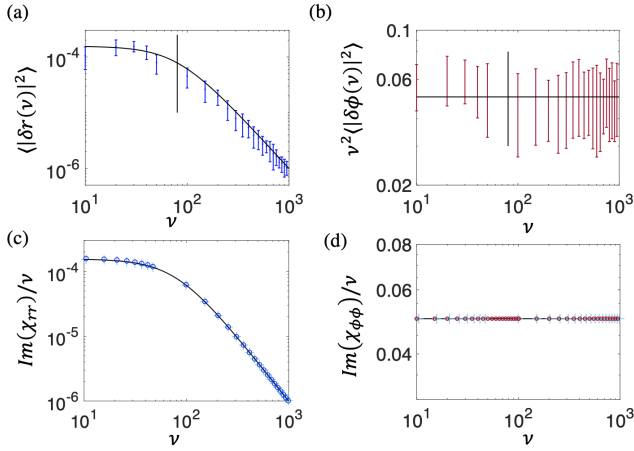


FIG. 9 (color online). **Correlation and response functions for the isochronous Hopf oscillator ( $b'' = 0$ )**: (a) Power spectral density of radial fluctuations as a function of frequency  $\nu$  (blue dots). (b) Phase diffusion constant, obtained from the product of the phase fluctuation power spectral density and  $\nu^2$  (red dots). In both panels, the vertical (black) line indicates the corner frequency of  $2\mu$ . (c) Response to  $f_r$  in the radial direction divided by frequency (light blue cross). (d) Response to  $f_\phi$  of the phase variable divided by frequency (light blue cross). Superposed on the panels (c, d) are predictions from the correlation functions of (a,b) depicted using open circles. Overlaid on all four plots are the respective theoretical predictions.

Eq. 18 was numerically computed using a random number generator that outputs a value in the range  $[0 - 1]$ . Comparison of this value with the occupation probabilities of the three states, determines the stochastic trajectory of each of the 50 particles. Further, since we define Fig. 4 in terms of transition rates, these probabilities are the product of the respective rates and a time step duration of  $10^{-2}$ . Lastly, while this isn't crucial to reproducing our results, all our particles in this dynamical system start with an initial state of -1. Data was always taken after running the system so that its initial conditions were no longer relevant. All simulations were performed in MATLAB (R2017a, the MathWorks, Natick, MA) and those for the discrete-time jump system will be made available on the author's Github page.

### Appendix C: Driven systems without adaptation

In the main text, we dive into two representative systems that incorporate an adaptive drive. For completeness we show results obtained from the Hopf system with a nonadaptive drive, *i.e.*, one with  $b'' = 0$ . This system without an adaptive drive admits a GFDT. In Fig. 9

we show that the response (black lines) and fluctuations (colored dots) agree as expected from the GFDT, or the FDT in the Frenet frame that is co-moving with the mean probability current in the driven oscillator. The fluctuations in the normal (radial) direction (blue) are still well

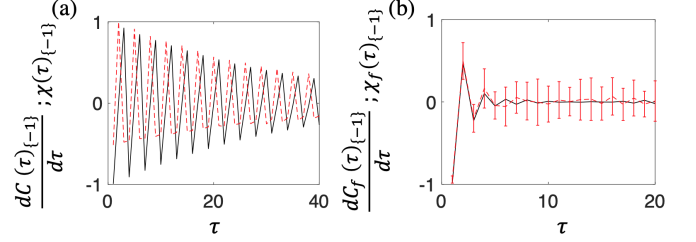


FIG. 10 (color online).  $\frac{dC}{d\tau}$  (**black solid**) vs  $\chi(\tau)$  (**red dashed**) for  $\alpha = 98$  and state  $\{-1\}$ : (a) Time derivative of the cross-correlation  $C_{-1,-1}$  and the response functions  $\chi_{-1,-1}$  superimposed illustrate the breakdown of FDT. (b) The Frenet frame formalism allows for the obedience of GFDT.

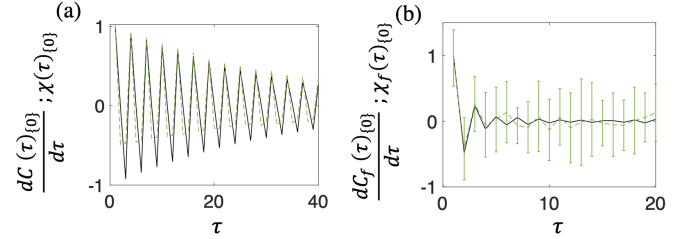


FIG. 11 (color online).  $\frac{dC}{d\tau}$  (**black solid**) vs  $\chi(\tau)$  (**green dashed**) for  $\alpha = 98$  for state  $\{0\}$ : Time derivative of the cross-correlation  $C_{0,-1}$  and response functions  $\chi_{0,-1}$  demonstrating violation of FDT in (a) and validity of GFDT in (b).

described by a simple Lorentzian (black), whose corner frequency is once again marked by a vertical line. However, the phase diffusion constant exhibits no frequency dependence (red) consistent with Eq. 14. Furthermore, the cross correlations  $C_{r\phi}$  vanish, and the responses depicted in subplots (c and d) agree that inferred from the GFDT and the correlation functions. When  $b$ , the hair cell model violates FD'T but obeys GFDT.

When examining the three-state system with broken detailed balance but no adaptation, we found that the GFDT holds as expected. In the main text we demonstrated the necessary correspondence for only one correlation function – see Fig. 6. For completeness, here we show the analogous results for states  $-1$  and  $0$  in Figs. 10 and 11 respectively. In all of these examples, the standard FDT breaks down, but the GFDT relations are valid.